pollutants

MDPI

Article

Multivariable 3D Geovisualization of Historic and Contemporary Lead Sediment Contamination in Lake Erie

K. Wayne Forsythe [1,2,*], Danielle E. Ford [1], Chris H. Marvin [3], Richard R. Shaker [1,2], Michael W. MacDonald [1] and Ryan Wilkinson [1]

[1] Department of Geography and Environmental Studies, Ryerson University, 350 Victoria Street, Toronto, ON M5B 2K3, Canada; dmitch@ryerson.ca (D.E.F.); rshaker@ryerson.ca (R.R.S.); mmacdon@ryerson.ca (M.W.M.); rwilkinson@ryerson.ca (R.W.)

[2] Graduate Program in Spatial Analysis, Department of Geography and Environmental Studies, and Graduate Programs in Environmental Applied Science and Management, Ryerson University, 350 Victoria Street, Toronto, ON M5B 2K3, Canada

[3] Aquatic Contaminants Research Division, Water Science and Technology Directorate, Environment and Climate Change Canada, Burlington, ON L7S 1A1, Canada; chris.marvin@canada.ca

* Correspondence: forsythe@geography.ryerson.ca

Abstract: Lead sediment contamination in Lake Erie stems from a long history of natural and synthetic resource production. Sediment samples with variable sampling densities were collected by the Canada Centre for Inland Waters in 1971, 1997/1998, and 2014. The kriging interpolation method was used to create continuous sediment contamination surfaces for time/space comparisons. Change detection analyses identified an overall decreasing trend in high lead pollution levels from 1971 to 2014, while sediments with the lowest concentrations increased in surface area. Lake-wide circulation patterns and bathymetric data were added to interpolated contamination surfaces to enhance the understanding of interrelated hydrodynamic processes and geophysical features in the movement of contaminated sediments. Utilizing visualization tools in Esri's ArcScene, bathymetric data were employed to enhance the geographic context of contamination maps. The physical barriers to sediment transportation created by bathymetric features can be visualized in three-dimensions. Elevated features between lake basins are easily recognized as impedances to lake currents when circulation directions are draped over the bathymetric model. By using illumination tools and techniques, geovisualizations of lead sediment contamination throughout Lake Erie create a scientific communication tool for a wide audience to use in multiple-criteria decision making for environmental remediation of sediment contamination.

Keywords: lead; kriging; 3D geovisualization; great lakes; sediment contamination; geostatistics; spatial analysis

Citation: Forsythe, K.W.; Ford, D.E.; Marvin, C.H.; Shaker, R.R.; MacDonald, M.W.; Wilkinson, R. Multivariable 3D Geovisualization of Historic and Contemporary Lead Sediment Contamination in Lake Erie. *Pollutants* **2021**, *1*, 29–50. https://doi.org/10.3390/pollutants1010004

Received: 29 January 2021
Accepted: 16 February 2021
Published: 21 February 2021

1. Introduction

The Great Lakes basin is an industrial, manufacturing, and agricultural powerhouse with a lengthy history of resource production. As one of the world's largest interconnected freshwater systems, the Great Lakes also provide fresh drinking water to over 30 million Canadians and Americans [1]. Lake Erie is the smallest Great Lake by volume at 484 km^3 [2]. It is surrounded by intensive farming activities, and several historically industrial cities (Detroit, MI, Windsor, ON, Toledo, OH, Cleveland, OH, Erie, PA, and Buffalo, NY, USA; Figure 1). Organic and inorganic contamination of Lake Erie has been an environmental concern since the mid-19th century [3]. Gradients toward decreasing sediment contamination from the western basin to the eastern basin of Lake Erie, and from the southern to the northern area of the central basin have been observed [4–7]. Toxic heavy metals, including lead (Pb), pose long-term risks of environmental contamination, as well as bioaccumulation in aquatic species [8–10]. When ingested by humans, Pb presents

critical behavioral, reproductive, and physiological health problems [11]. Since 1990, both Canada and the United States have banned the use of leaded gasoline under the Canadian Environmental Protection Act [12] and the Clean Air Act [13] resulting in fewer cases of human Pb poisoning [11].

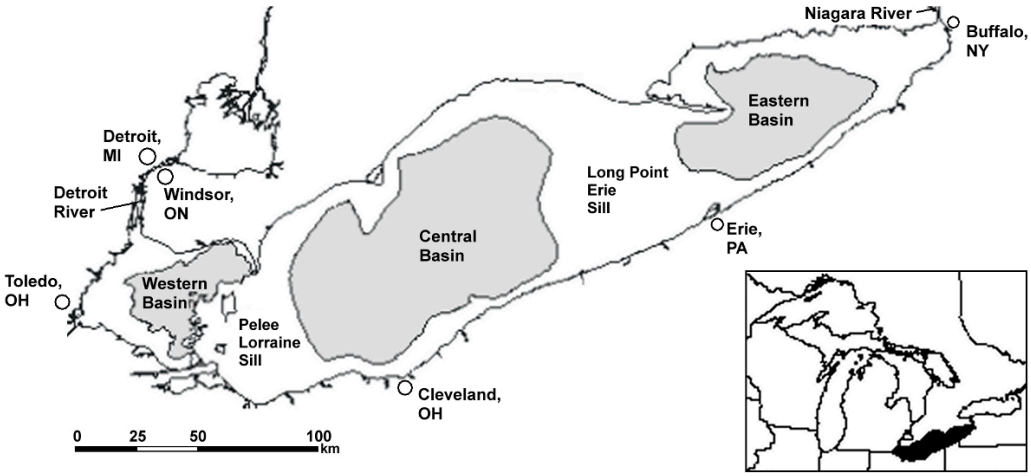

Figure 1. Location of Lake Erie and its major depositional basins, source: modified after [4,7,14].

Hydrodynamic conditions and bathymetric contours influence the spatial patterns of Pb sediment contamination throughout Lake Erie. Until recently, visualizations of sediment contamination [14] and internal lake processes [15] were presented in two-dimensions (2D). In 2014, the National Oceanic and Atmospheric Administration (NOAA) introduced a complete bathymetric model of Lake Erie and its basin [16] (Figure 2). Hundreds of thousands of soundings measurements collected for over 100 years by the U.S. Army Corps of Engineers, the NOAA Coast Survey, and the Canadian Hydrographic Service were compiled to create the Bathymetry of Lake Erie and Lake Saint Clair [16].

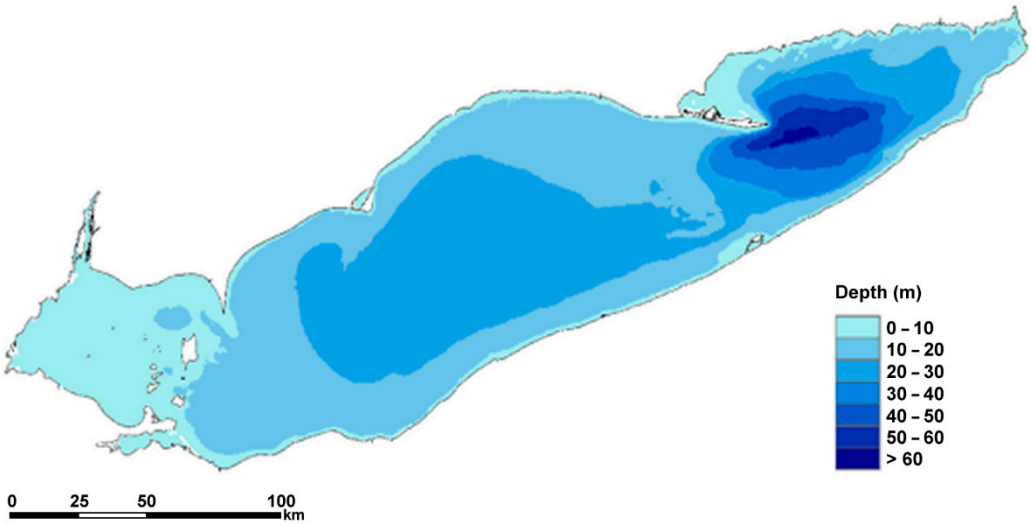

Figure 2. Lake Erie depth (m).

The innovative bathymetric model allows for the dynamic relationship between sediment contamination and lake circulation patterns to be visualized in three-dimensions (3D). This research intends to produce novel 3D geographic visualizations of Pb sediment contamination from 1971, 1997/1998, and 2014 for two purposes; to increase the spatial awareness of sediment contamination patterns over time, and to create approachable yet valuable pollution maps to be interpreted by a wide variety of users for remediation decision making.

1.1. Pb Contamination in Lake Erie

Environmental Pb contamination stems primarily from anthropogenic sources including agricultural pesticide and fertilizer use [8], industrial manufacturing of batteries, and air pollution from fossil fuel combustion [8,10,11,17]. Sediments reflect differing sources of anthropogenic Pb superimposed on the natural component such as regional deforestation from 1860 to 1890, followed by coal combustion and ore smelting through 1930. From 1930 to 1980, the combustion of leaded gasoline was the most dominant anthropogenic source of lead contamination to the atmosphere, and by inference, lake sediments. After the abolishment of leaded gasoline, industry became the dominant anthropogenic source [18]. Anthropogenic Pb pollution is known to have a strong affinity for clay sediments [10,19,20]. Naturally occurring Pb is minimal at background levels of 18.2 μg/g [21,22]. Trace levels in the natural environment originate from volcanic eruptions and erosion of crustal rock containing Pb minerals [22].

1.2. Lake Erie Circulation

Hydrodynamic processes underlie most lake-wide physical and biological activities [23]. Waves, currents, and circulation patterns influence the distribution and displacement of sediments, as well as the rate at which contamination is transported throughout the basin [15,17,23,24]. Episodic waves created during storm events have a greater impact on the movement of sediments in the nearshore coastal zone (0–20 m deep, Figure 2) than average climatic conditions [25] and circulation throughout the lake [24,26]. A rise in major storms and weather extremes resulting from climate change are anticipated to impact the biophysical characteristics and hydrodynamic processes of the Great Lakes basin [26–29]. For example, less lake-wide ice coverage throughout the winter months may lengthen the Great Lakes storm season, ultimately exposing vulnerable coastal regions to more frequent opportunities for sediment resuspension [25].

Prevailing westerly winds, parallel to the basin's orientation, are largely responsible for the annual circulation patterns of Lake Erie [15,23] (Figure 3). This strong, consistent wind creates a counter-rotating two-gyre circulation system within the relatively flat bathymetry of the central basin [23,30]. Lake Erie is the shallowest Great Lake averaging 19 m deep, reaching a maximum of 64 m in the eastern basin [2]. Strong currents flow along the shallow shorelines with the prevailing westerly winds [23,30] reaching upwards of 3.7 cm/s along the Ohio shoreline near Cleveland [15]. Pressure gradients drive the westward flow in deep offshore regions of the central basin [15] creating an anticyclonic gyre (Figure 3a) along the Ontario shoreline and a cyclonic gyre (Figure 3b) along the Ohio shoreline.

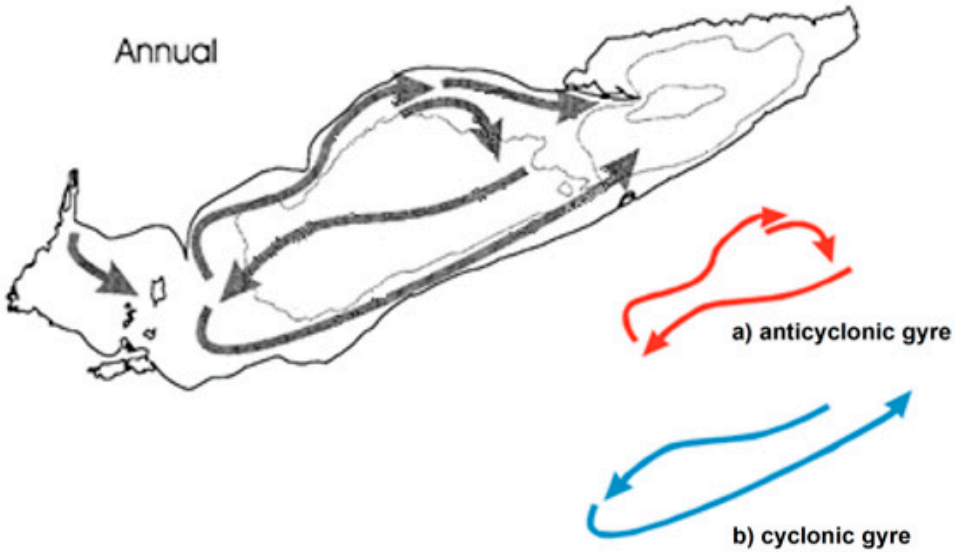

Figure 3. Annual Lake Erie circulation patterns with 20 m and 50 m bathymetry isolines [15]; the two-gyre system in the central basin is identified individually by the (**a**) anticyclonic gyre and (**b**) cyclonic gyre.

Stronger wind-driven currents and waves can develop over the central basin due to the flat and shallow nature of the basin bathymetry [15,31]. With few physical impedances to reduce wind stresses, the central basin is vulnerable to frequent sediment resuspension [26,32,33]. At a maximum depth of 23.5 m, the central basin is almost entirely classified within the coastal zone (<20 m), where wind-driven wave activity fosters sediment resuspension and transportation [25,32]. The shorelines of Lake Erie are also defined by very steep slopes (>45 degrees) and shallow littoral zones [34,35]. Fine-grained sediment substrates most vulnerable to erosion and transportation (i.e., clay, silt, and sand) dominate the southern shoreline where wind-driven currents are strongest [15]. Sediments in the littoral zone are more likely to be resuspended and transported by wave action [35], especially on steep slopes where unconsolidated sediments are vulnerable to gravitational and erosional processes [36].

1.3. Geovisualization

The term "geovisualization" is a product of Visualization in Scientific Computing by McCormick et al. [37]. Geovisualization is a method of displaying geographic data, or thematic information as a visual tool for exploratory data analysis (EDA), knowledge construction and decision making [38–40]. When employed under data analysis conditions other than EDA, Rinner [41] suggests the term "visual analytics" as a more appropriate name for the visualization of processed data. Regardless of the stage in which geovisualizations are employed, Andrienko and Andrienko [38], and Ruda [42] recommend its integration with multiple-criteria decision making (MCDM).

Visualizing geographic data as maps or graphs illustrates spatial trends, patterns, and relationships between multivariate and multidimensional geographic processes and phenomena [40,41,43]. When available, digital elevation models (DEM) and bathymetric data can enhance the perception of spatial data patterns within their geographic context [41,44,45]. This degree of perception (especially of geometric shapes and contours) can be illuminated by 3D visualization tools (i.e., hillshade) and lighting effects [45]. By effectively draping thematic data layers (of sediment contamination, for example) onto 3D geographic contours, complex multivariate data analyses are possible through a novel, yet approachable illustration of spatial data interacting with underlying geomorphological processes [40,44].

2. Data

The Great Lakes Basin Sediment Database (Environment and Climate Change Canada) houses sediment surveys conducted by the Water Science and Technology Directorate (previously the National Water Research Institute) and the Great Lakes Surface Water Surveillance Program [4,46] since 1965. Sediment contamination in Lake Erie was first sampled in 1971 (263 survey locations) in a grid fashion with survey locations spaced 10 km apart, and again in 1997/1998 (55 survey locations) and 2014 (34 survey locations). The drastic change in survey density was the result of increasing procedural costs between the three sampling periods. The 2014 survey locations were randomly selected and mostly located in deep offshore regions of the lake [5,6,47]. Similar contaminated sediment distribution analyses in Lake Erie showed that offshore depositional basins were generally more polluted. The sediment sampling locations for the most recent survey considered both the reduction in historical contaminant loadings and accounted for increasingly diffuse open-lake pollutant distributions [5,6]. Descriptive statistics for each sediment survey are presented in Table 1.

Table 1. Descriptive statistics of Pb sediment contamination samples from Lake Erie.

Year	Minimum (µg/g)	Maximum (µg/g)	Mean (µg/g)	Standard Deviation	Variance
1971	9.30	299.30	85.98	49.55	2455.20
1997/1998	4.98	104.27	43.08	23.21	538.70
2014	5.00	168.00	40.61	27.49	755.70

2.1. Kriging

Kriging is a geostatistical method of spatial interpolation used to estimate contamination values at unsampled locations from existing sample measurements [48,49]. This mathematical tool is utilized to transform discrete Pb contamination measures into a continuous data layer. In doing so, sediment surveys of different point densities and from different collection periods can be more accurately compared over space and time. Kriging also produces valuable cross-validation statistics describing the validity of a predictive model in accurately estimating contamination values at unsampled locations [47,50,51].

Conventional standards of a statistically valid, unbiased kriging model include a Mean Prediction Error (MPE) close to 0, an Average Standard Error (ASE) less than 20, a Standardized Root-Mean-Squared Prediction Error (SRMSPE) close to 1, and a minimal difference between the Root-Mean-Squared Prediction Error (RMSPE), and ASE [52–57]. In addition to estimating values at unsampled locations, kriging interpolation also predicts a value at all sampled locations from which the model is identified to underestimate (MPE > 0) or overestimate (MPE < 0) existing measurements [51,58]. Under- or overestimation of variability made by the kriging model is also represented by SRMSPE values greater than or less than 1 µg/g, respectively [52,55–57].

2.2. Canadian Sediment Quality Guidelines for the Protection of Aquatic Life

The degrees of Pb sediment contamination that threaten the health and biological well-being of humans and aquatic life have been established by the Canadian Council of Ministers of the Environment [49,59]. The Threshold Effect Level (TEL) for Pb contamination is 35.00 µg/g (CCME, 1999). Below this level of pollution, biological risks to humans and aquatic life are not likely to occur [49]. The Probable Effect Level (PEL) for Pb contamination is 91.30 µg/g [59]. Above this level, biological risks to humans and aquatic life are expected to frequently occur [49]. Sediment contamination with respect to the TEL and PEL should be monitored over time for potential changes in concentrations.

3. Methods

3.1. Kriging Geostatistical Interpolation

During preliminary data exploration, Pb samples from 1971, 1997/1998, and 2014 were identified to be abnormally distributed from histogram analyses. Kriging cross-validation errors (RMSPE and ASE) at or exceeding their respective conventional standards of statistical validity (Table 2) also suggested abnormally distributed data. Similar geospatial analyses of sediment contamination [48,60,61] recommend a log-transformation of abnormally distributed data sets to improve the accuracy and statistical validity of kriging procedures (Table 3).

The three datasets were best modelled using an exponential distribution, and the parameters are listed in Table 4. The kriging analysis was set to include a minimum of one (1) and a maximum of five (5) neighbors as influential points in predicting values at unsampled locations. Selecting the most appropriate distribution model was determined through an experimental assessment of different parameter combinations and their respective cross-validation statistics. All kriging models produced SRMSPE values close to 1, and low (~0) MPE and ASE values [14] (Table 3).

Table 2. Kriging cross-validation statistics of the 1971, 1997/1998, and 2014 Pb datasets.

Year	MPE (µg/g)	RMSPE (µg/g)	SRMSPE (µg/g)	ASE (µg/g)	RMSPE-ASE (µg/g)
1971	0.508	31.803	0.919	34.699	−2.896
1997/1998	0.482	19.399	0.969	20.592	−1.193
2014	−0.597	27.107	1029	23.511	3.596

Table 3. Kriging (log-normal) cross-validation statistics of the 1971, 1997/1998, and 2014 Pb datasets.

Year	MPE (µg/g)	RMSPE (µg/g)	SRMSPE (µg/g)	ASE (µg/g)	RMSPE-ASE (µg/g)
1971	0.003	0.189	1.033	0.181	0.008
1997/1998	0.011	0.258	1.062	0.251	0.007
2014	0.008	0.248	1.014	0.238	0.010

Table 4. Kriging parameters used for modelling the 1971, 1997/1998, and 2014 Pb (log-normal) datasets.

Year	Distribution Model	Major Range (m)	Minor Range (m)	Direction (°)	Lag Distance
1971	Exponential	100,000	50,000	90	30,832
1997/1998	Exponential	100,000	50,000	90	28,552
2014	Exponential	100,000	50,000	90	27,086

3.2. 3D Geovisualization

Lake Erie bathymetric data were acquired in an ARC ASCII file format from the NOAA National Centers for Environmental Information (NCEI). This DEM contains both terrestrial elevation and bathymetric data of Lake Erie and its basin. First, bathymetric data were extracted from the DEM by the surface extent of Lake Erie. A depth profile chart was created using ArcMap's 3D Analyst [62] for preliminary analysis of lake depth across the basin (Figure 4).

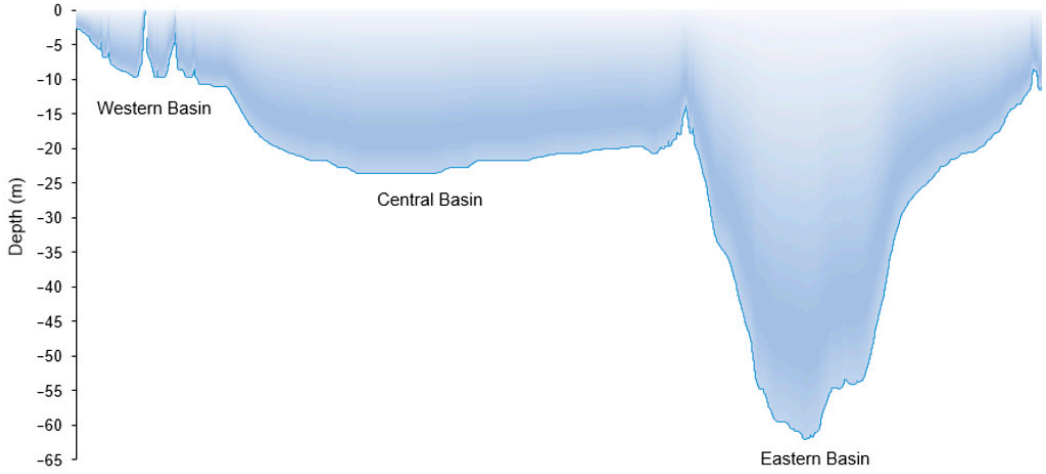

Figure 4. Lake Erie depth profile in meters from west to east.

Esri's 3D viewing application ArcScene [62] was used to create geovisualizations of Pb contamination throughout Lake Erie. This program displays elevation data (Z) from feature geometry and allows for the 3D geovisualization of thematic data layers [62]. Average annual lake-wide circulation patterns were digitized (based on maps by Beletsky et al. [15] and integrated into 3D geovisualizations of Pb sediment contamination patterns. Along with bathymetric data, circulation patterns provide a hydrodynamic context to sediment movement throughout the basins of Lake Erie.

The bathymetry of Lake Erie is displayed in Figures 5 and 6. The crescent-shaped ridges created by the Long Point-Erie Sill and the Long Point Spit extending into the eastern basin overshadow deeper contours when viewed from the normal southern position (Figure 5). Various viewing perspectives were examined to provide the best overall lake bathymetry visualization while also fully portraying the variation in contamination surfaces. The lake viewpoint was therefore rotated to the southeast perspective (Figure 6) to best view the complex shape and contours of the eastern basin and to provide the best viewpoint for 3D geovisualization [56].

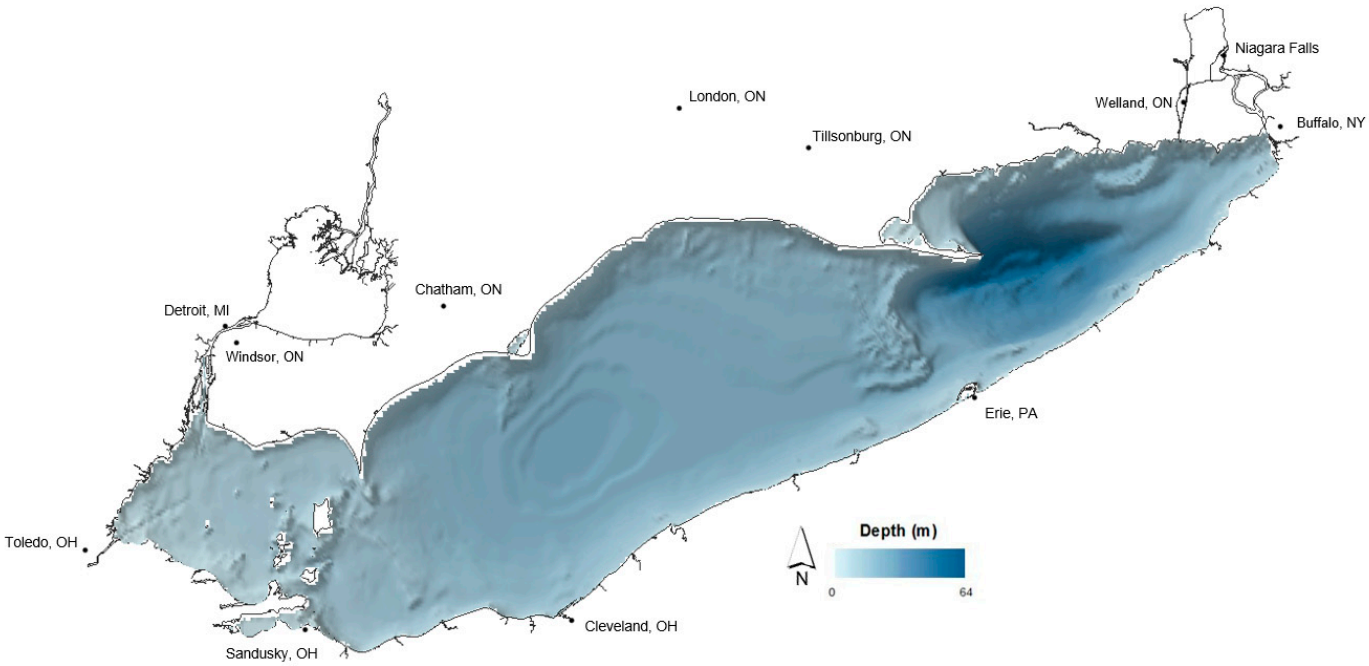

Figure 5. Bathymetry of Lake Erie viewed from the normal southern position.

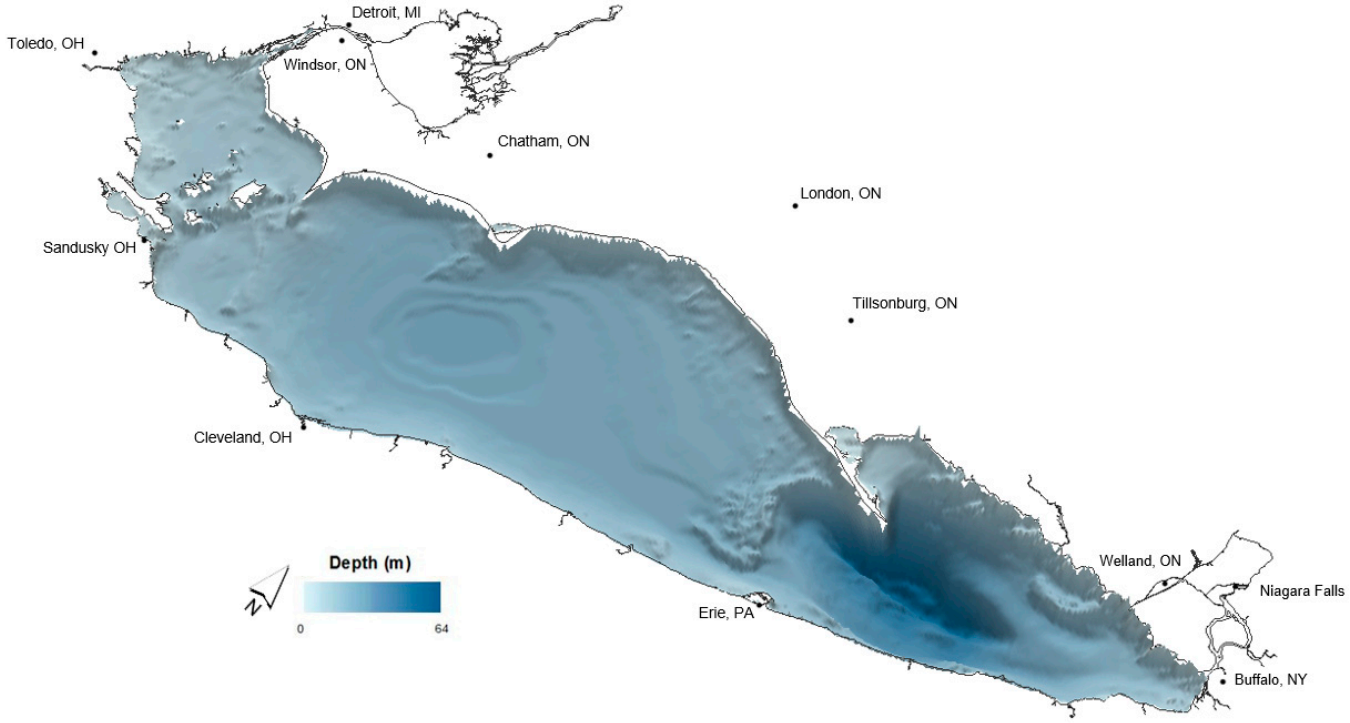

Figure 6. Bathymetry of Lake Erie from the southeast perspective.

3.3. Change Detection

Change detection analyses were performed between each survey period (1971 and 1997/1998, 1997/1998 and 2014, and 1971 and 2014) to assess the degree and spatial extent of Pb sediment contamination change over time. Contamination intervals in each map were aggregated to <TEL, ≥TEL to <PEL, and ≥PEL categories to simplify the change detection output (Table 5). These intervals were then reclassified in each contamination map to unique numeric identifiers, which when added together, identified the degree of contamination change between the three survey periods. Each possible degree of change between two Pb contamination maps is displayed and described in Table 6.

Table 5. Pb (log-normal) contamination intervals <TEL, ≥TEL to <PEL, and ≥PEL.

Contamination Intervals <TEL (µg/g)	Contamination Intervals ≥TEL to <PEL (µg/g)	Contamination Intervals ≥PEL (µg/g)
0.00 to <11.67	≥35.00 to <53.77	≥91.30 to <110.07
≥11.67 to <23.33	≥53.77 to <72.53	≥110.07 to <128.83
≥23.33 to <35.00	≥72.53 to <91.30	≥128.83

Table 6. Contamination change categories and their meanings.

Change Category	Description
101	No change, <TEL
102	<TEL to ≥TEL to <PEL
103	<TEL to ≥PEL
201	≥TEL to <PEL to <TEL
202	No change, ≥TEL to <PEL
203	≥TEL to <PEL to ≥PEL
301	≥PEL to <TEL
302	≥PEL to ≥TEL to <PEL
303	No Change, ≥PEL

4. Spatial Analysis

4.1. Kriging Results

The spatial extent of Pb contamination from 1971, 1997/1998, and 2014 sediment surveys are presented in Table 7 and Figures 7–9. In 1971, contamination ≥PEL covered 37.92% of the study area (24,983.5 km^2) and was mostly found at the mouth of the Detroit River and along the shoreline of Ohio, following the direction of the strongest annual circulation pattern (Figure 7). From this survey, high Pb sediment contamination did not necessarily correlate with depth. Contamination ≥128.83 µg/g was estimated in sediments throughout the shallow western and central basins. In the deepest contours of the eastern basin, the maximum predicted Pb contamination ranged from 91.30 to <128.83 µg/g.

Table 7. Spatial extent of predicted Pb (log-normal) contamination by year.

Year	Area	<TEL	≥TEL to <PEL	≥PEL	Total Analysis Area	No Data
1971	km^2	3347.5	12,162.25	9473.75	24,983.5	816.5
	%	13.4	48.68	37.92	96.84	3.16
1997/98	km^2	11,313.5	13,205	n/a	24,518.5	1281.5
	%	46.14	53.86	n/a	95.03	4.97
2014	km^2	9964.5	13,134.75	182.25	23,281.5	2518.5
	%	42.8	56.42	0.78	90.24	10.82

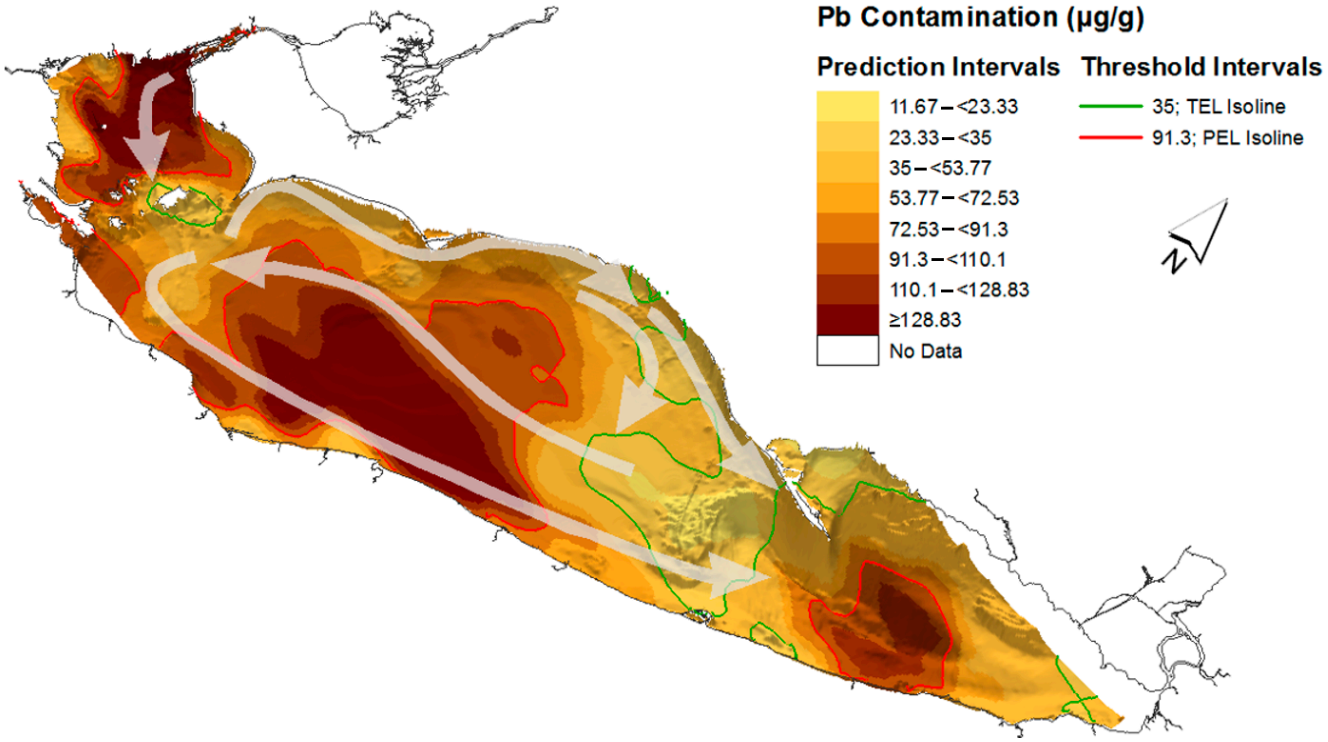

Figure 7. Kriging results of the 1971 Pb (log-normal) contamination in Lake Erie with average annual circulation patterns.

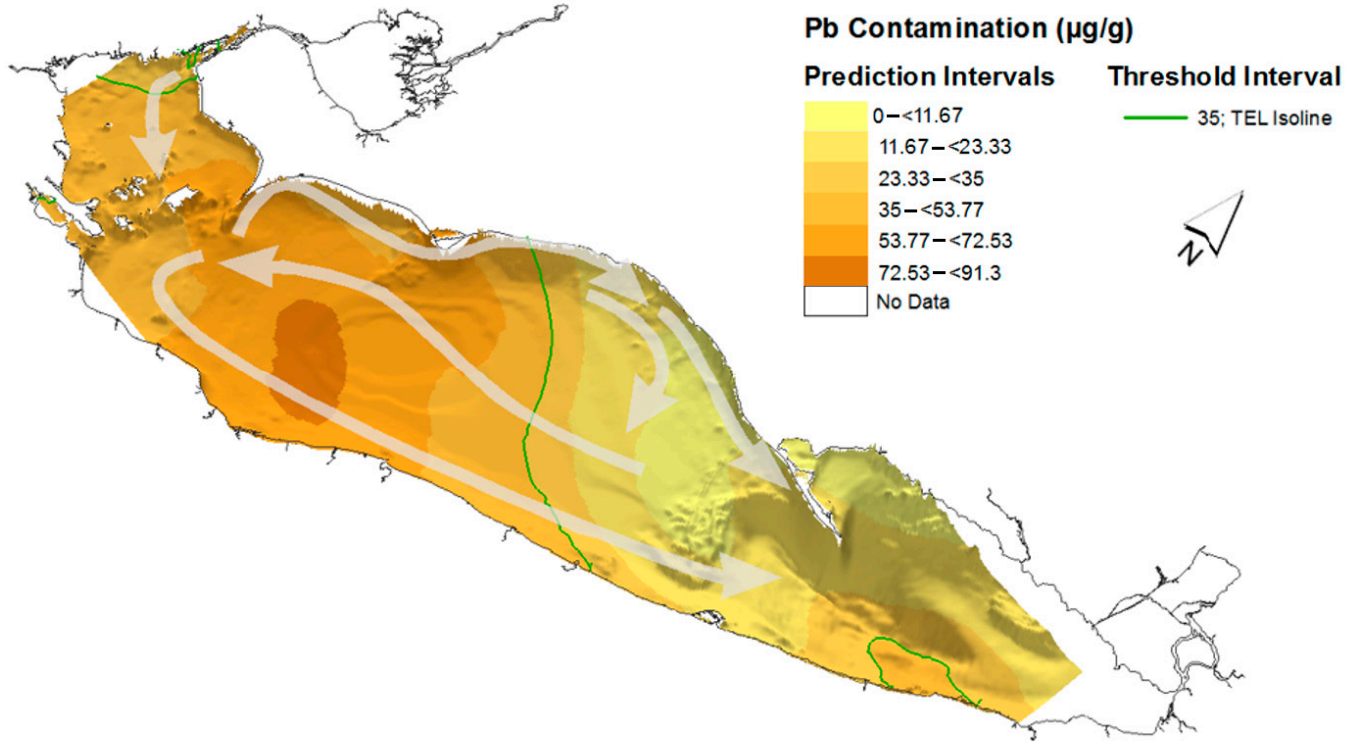

Figure 8. Kriging results of the 1997/1998 Pb (log-normal) contamination in Lake Erie with average annual circulation patterns.

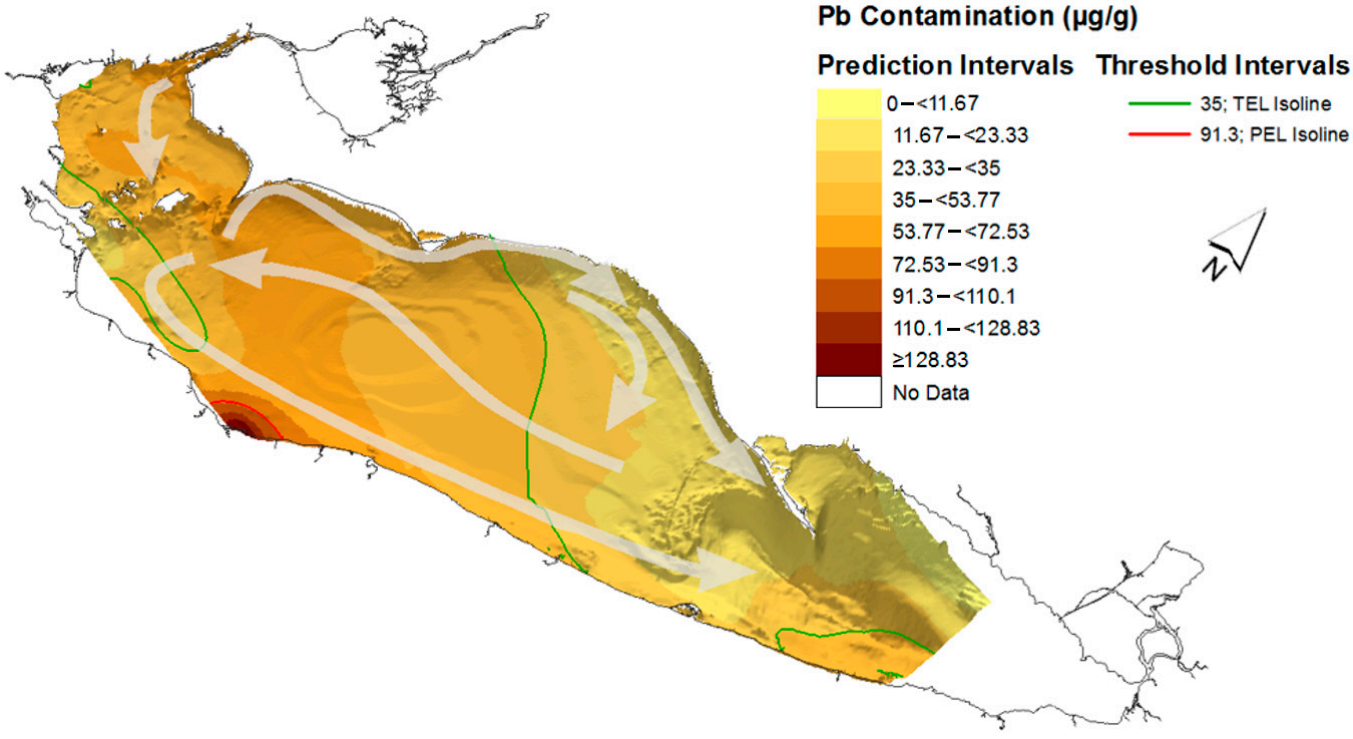

Figure 9. Kriging results of the 2014 Pb (log-normal) contamination in Lake Erie with average annual circulation patterns.

Nearly half (48.68%) of the study area along the northern (Ontario) shoreline, and throughout the central and eastern basins was predicted to have Pb contamination levels ≥TEL to <PEL from the 1971 sediment survey. Sediments surrounding Pelee Island in the western basin and along the Long Point-Erie sill in the central basin were predicted to have the least amount of Pb contamination (13.4%). Pb contamination ranging from <PEL generally aligned with the northeast circulation patterns parallel to the Ontario shoreline from Pelee Island to the Long Point-Erie Sill [32]. Due to the sediment survey point distribution, some areas of Lake Erie were excluded from the prediction surface. The 1971 dataset allowed for 96.84% of the 25,800 km^2 lake surface area to be mapped by the kriging prediction model, leaving 8165 km^2 of Lake Erie classified as No Data.

Lake Erie sediment contamination did not exceed the PEL in 1997/1998 (Figure 8). The TEL isoline roughly divided the lake in half through the central basin; contamination ≥TEL to <PEL to the west and <TEL to the east. Pb Contamination ≥TEL to <PEL had advanced further towards the eastern basin along the southern shoreline than contaminated sediments to the north. Specifically, 53.86% and 46.14% of Pb contamination from the 1997/1998 survey was predicted to range from ≥TEL to <PEL and <TEL, respectively. Due to the lower point density and distribution of the 1997/1998 survey samples, 95.03% of the study area was included in the kriging analysis. The utilization of the kriging technique allows for patterns to be examined on a lake-wide basis. It is also useful when comparing sediment surveys where different sampling strategies are employed over time.

The 2014 sediment survey produced contamination prediction patterns similar to those estimated from the 1997/1998 dataset (Figure 9). One notable difference is the small portion (0.78% of the study area) of Pb sediment contamination outside of Cleveland, OH. The TEL isoline created a similar division of the lake to that of the 1997/1998 TEL isoline. However, the 2014 dataset estimated slightly more area (56.42%) represented by Pb contamination ≥TEL to <PEL throughout all three basins. Like the 1997/1998 map, contamination ≥TEL to <PEL in the central basin had advanced further eastward along the southern shoreline, following the strong circulation patterns in this region of the lake. Sediment contamination <TEL was predicted to represent 42.8% of the study area predominately in the central and eastern basins along the Ontario shoreline and the Long Point-Erie Sill. The 2014 dataset contained the fewest sampling point locations of the three surveys resulting in the smallest area of analysis at 23,281.5 km^2 (90.24% of the lake surface area).

4.2. Spatiotemporal Change in Pb Sediment Contamination

The degree of change in sediment contamination between 1971 and 1997/1998 is displayed in Figure 10. Between both sediment surveys (~27 years apart), more than half (65%) of the lake study area experienced a decline in sediment contamination levels (Table 8). Throughout most of the western and central basins (33.41% of the study area), Pb contamination levels ≥PEL in 1971 decreased to ≥TEL to <PEL by 1997/1998. At the mouth of the Detroit River, and in small sections of the central and eastern basins (5.34% of the study area), contaminated sediments ≥PEL in 1971 were drastically reduced to <TEL by 1997/1998. Throughout the eastern half of the central basin and the eastern basin (26.26% of the study area), Pb sediment contamination decreased from ≥TEL to <PEL to <TEL between the two survey periods. The only instance of increased Pb contamination between 1971 and 1997/1998 was in sediments surrounding Pelee Island along the Pelee-Lorraine Sill (0.72% of the study area). The remaining 34.28% of lake study area identified sediments that did not experience any degree of contamination change (based on threshold intervals) between 1971 and 1997/1998. Pb contamination ≥TEL to <PEL remained throughout the western and central basins (21.72% of the study area); along the Ontario shoreline in the central basin and the Long Point-Erie Sill sediment contamination remained at <TEL from 1971 to 1997/1998.

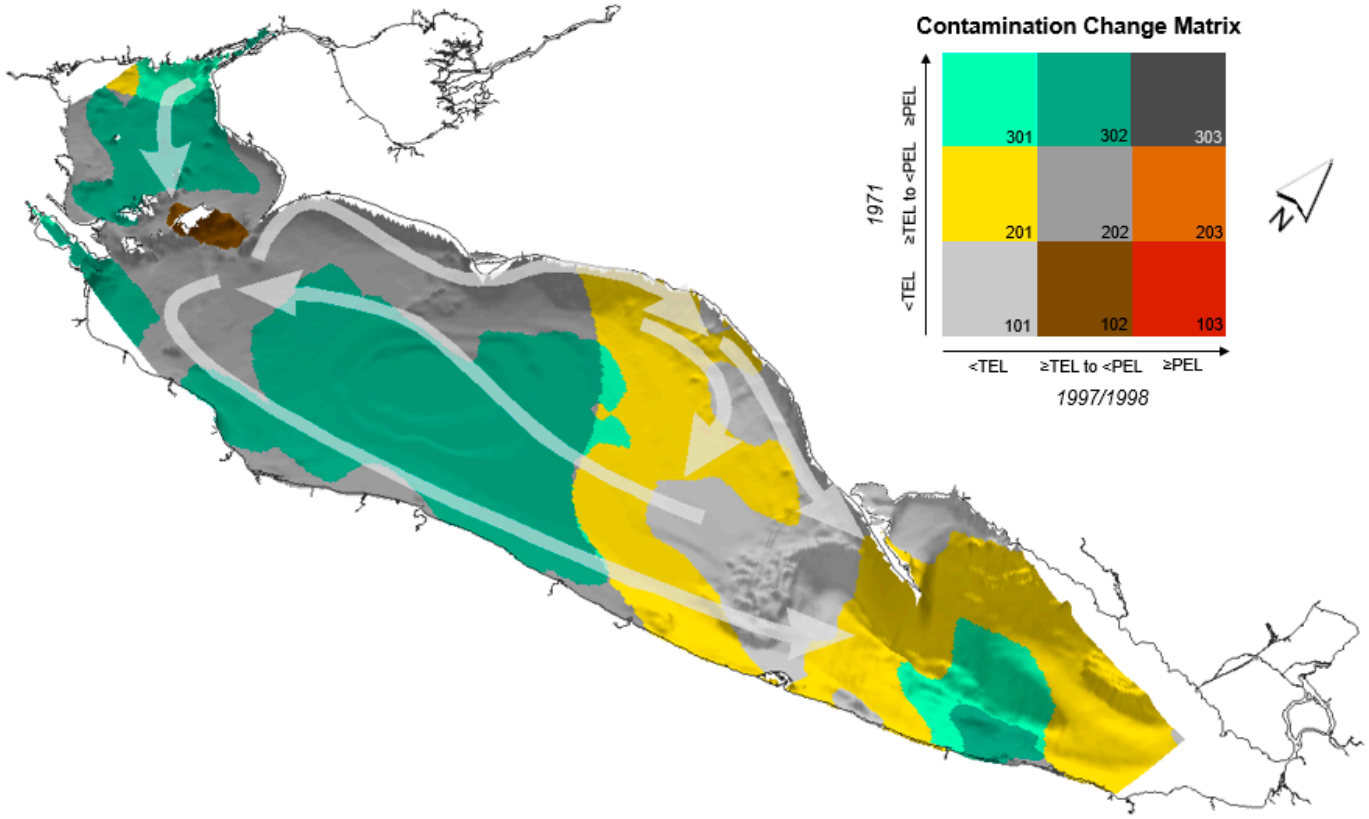

Figure 10. Change in Pb (log-normal) sediment contamination between 1971 and 1997/1998.

Table 8. Surface area change in Pb (log-normal) sediment contamination between 1971 and 1997/1998.

Change Category	Description	Area (km^2)	Area (%)
101	No Change, <TEL	3060.5	12.55
102	<TEL to ≥TEL to <PEL	175	0.72
201	≥TEL to <PEL to <TEL	6404.75	26.26
202	No change, ≥TEL to <PEL	5297.25	21.72
301	≥ PEL to <TEL	1302.75	5.34
302	≥ PEL to ≥TEL to <PEL	8146.5	33.41
No Data		1413.25	5.8

Concentrations of Pb sediment contamination in Lake Erie remained relatively stable between 1997/1998 and 2014 (Figure 11). Contamination measures throughout most of the study area (90.11%) did not change in the 17 years between surveys (Table 9). More than half (51.66%) of the sediments maintained contamination values ranging from ≥TEL to <PEL throughout the western basin and half of the central basin. A distinct boundary runs through the middle of the central basin, where sediment contamination to the east and extending into the eastern basin remained at <TEL between 1997/1998 and 2014 (representing 38.44% of the study area). Only 9.89% of the lake study area experienced a change in Pb sediment contamination between the two surveys. A small area (182 km^2) outside of Cleveland saw an increase in Pb sediment contamination values, ranging from ≥TEL to <PEL in 1997/1998 to ≥PEL by 2014. Sediment contamination also worsened at the mouth of the Detroit River and in small sections of the central and eastern basins where Pb measured <TEL in 1997/1998 up to ≥TEL to <PEL in 2014. This change in the central basin suggests an eastward expansion of contaminated sediments ranging from ≥TEL to <PEL. This contamination threshold boundary also identifies a small proportion of contaminated sediments closest to the Ontario shoreline, which have improved between the two surveys. Here, as well as along the Ohio shoreline in the western and central basins,

Pb contamination values have fallen from ≥TEL to <PEL in 1997/1998 to <TEL in 2014 (representing a total of 1023 km^2).

Change in Pb sediment contamination between historic (1971) and contemporary (2014) surveys detail a complex history of pollution in Lake Erie (Figure 12). Approximately 15,466 km^2 of the lake study area experienced a change in Pb sediment contamination values between 1971 and 2014 (Table 10); 97.75% of which represented a decline in Pb contamination levels.

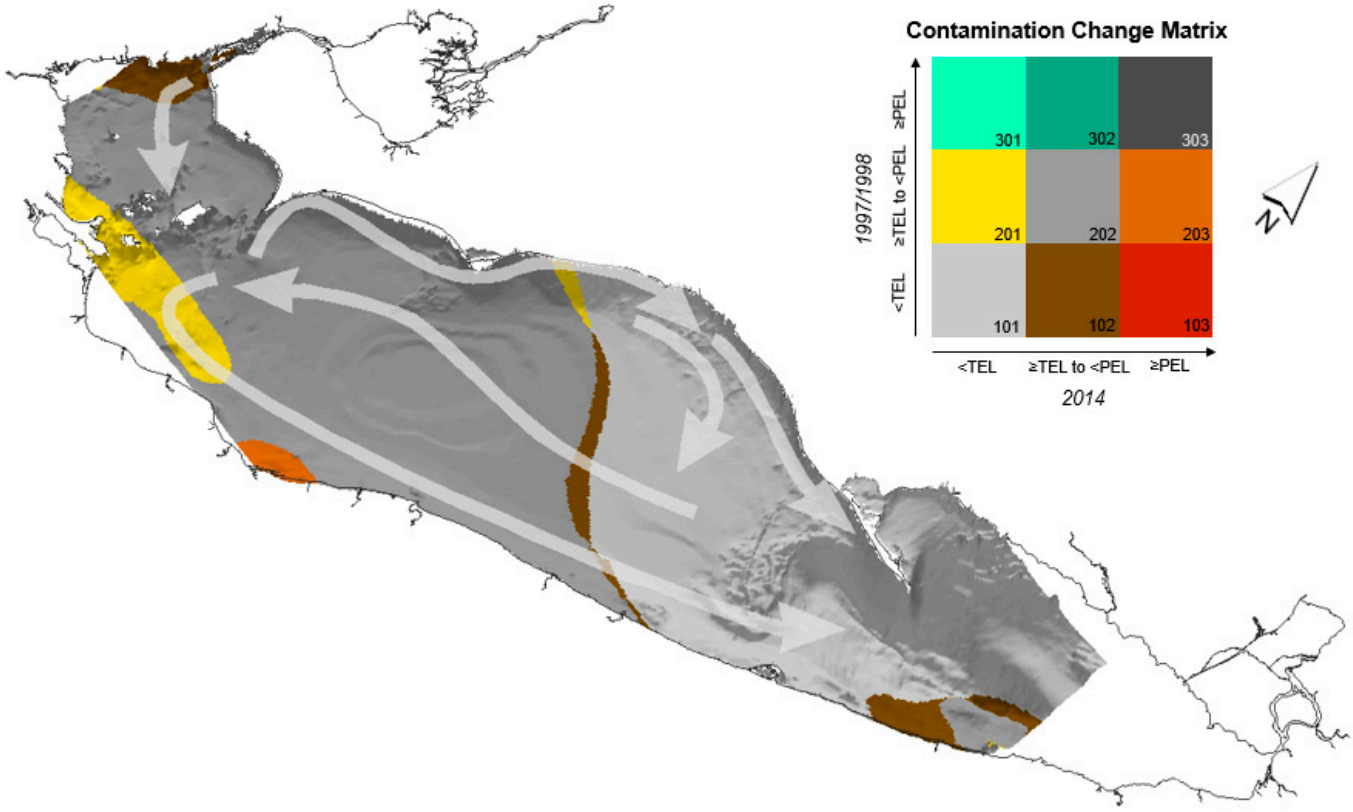

Figure 11. Change in Pb (log-normal) sediment contamination between 1997/1998 and 2014.

Table 9. Surface area change in Pb (log-normal) sediment contamination between 1997/1998 and 2014.

Change Category	Description	Area (km^2)	Area (%)
101	No Change, <TEL	8913.75	38.44
102	<TEL to ≥TEL to <PEL	1088.75	4.70
201	≥TEL to <PEL to <TEL	1023	4.41
202	No change, ≥TEL to <PEL	11,979.25	51.66
203	≥TEL to <PEL to ≥PEL	182	0.78
No Data		2613.25	11.27

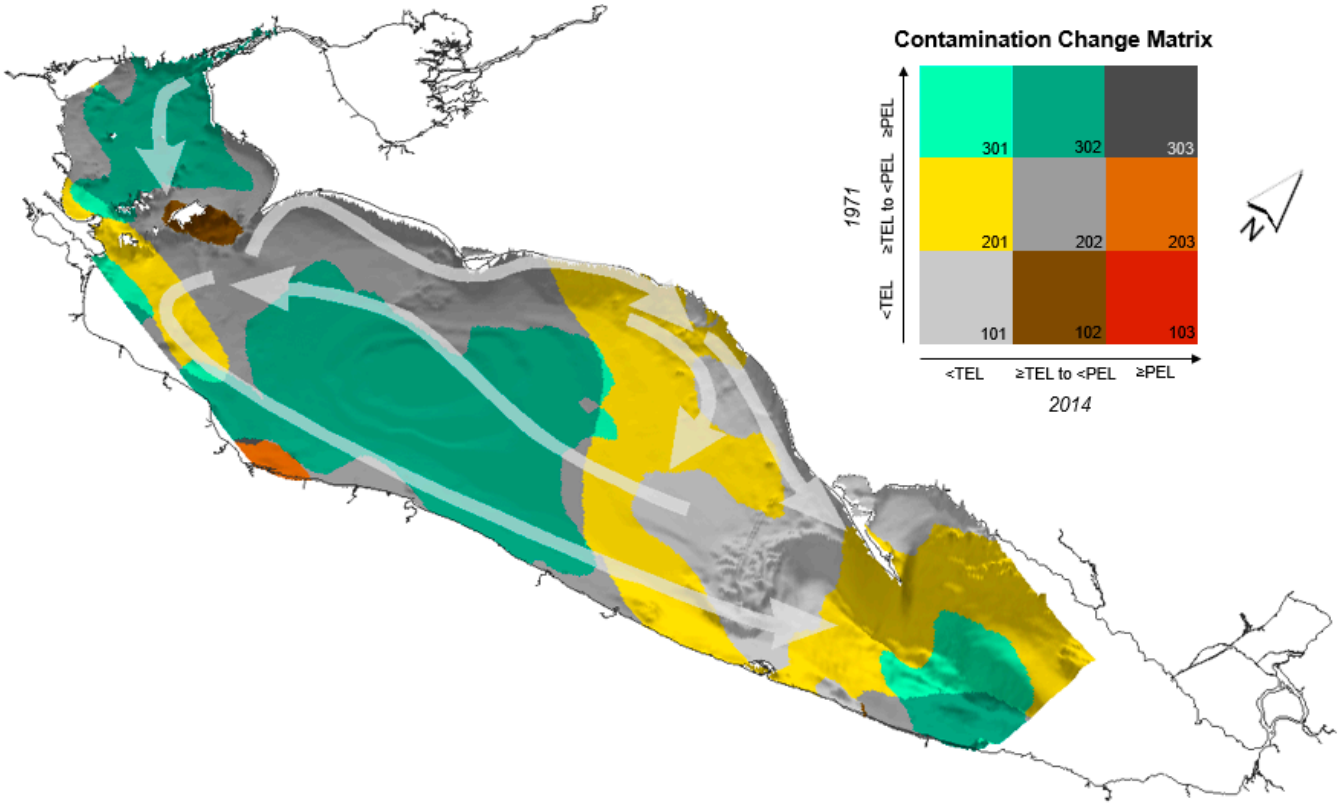

Figure 12. Change in Pb (log-normal) sediment contamination between 1971 and 2014.

Table 10. Surface area change in Pb (log-normal) sediment contamination between 1971 and 2014.

Change Category	Description	Area (km^2)	Area (%)
101	No Change, <TEL	3048.25	13.13
102	<TEL to ≥TEL to <PEL	179.5	0.77
201	≥TEL to <PEL to <TEL	5964	25.69
202	No change, ≥TEL to <PEL	4692.5	20.21
203	≥TEL to <PEL to ≥PEL	167.5	0.72
301	≥PEL to <TEL	925	3.98
302	≥PEL to ≥TEL to <PEL	8230	35.45
303	No Change, ≥PEL	12.25	0.05
No Data		2581	11.12

Pb contamination ≥PEL in 1971 was widely reduced by 2014 where 8230 km^2 of the study area declined to measures between ≥TEL to <PEL, and 925 km^2 were dramatically lowered to <TEL. Sediments ranging in contamination ≥TEL to <PEL were also largely reduced to <TEL values throughout all three basins. Approximately 33% of the lake study area did not experience change in Pb contamination levels between 1971 and 2014. A very small area (12.25 km^2) outside of Cleveland measured contaminated sediments ≥TEL in both 1971 and 2014. Contamination ≥TEL to <PEL remained largely in the western and central basins, whereas <TEL contamination persisted in the central and eastern basins between the two surveys.

Discrete areas of sediment in Lake Erie became more polluted between 1971 and 2014. Outside of Cleveland, an area of 1675 km^2 increased in Pb sediment contamination from ≥TEL to <PEL in 1971 to ≥PEL by 2014. Around Pelee Island and the Pelee-Lorraine Sill, sediments increased in Pb contamination from <TEL in 1971 to ≥TEL to <PEL (representing 1795 km^2 of the study area) by 2014. Increasingly contaminated sediments only represented an area of 347 km^2 or 1.5% of the lake study area between 1971 and 2014.

5. Discussion

5.1. Historic and Contemporary Pb Sediment Contamination

Assessing interpolated surfaces of historic and contemporary sediment surveys identified fluctuating conditions of Pb sediment contamination throughout Lake Erie over both space and time. An overall trend of decreasing contamination at the ≥PEL threshold occurred over the survey periods. Throughout the entire lake, contaminated sediments ≥PEL had decreased in surface area from 1971 (36.72%) to 1997/1998 (0%) to 2014 (0.71%). By 2014, sediment contamination ≥PEL had changed from a lake-wide problem to a localized condition outside of Cleveland. The relatively unchanging state of Pb sediment contamination from ≥TEL to <PEL is concerning, considering its high proportional representation of lake surface area almost exclusively in the western portion of the lake near highly urbanized and industrialized cities. Sediments contaminated to Pb levels <TEL fluctuated between sediment surveys. In 1971, only 12.97% of the entire lake area was represented by sediments <TEL; this extent more than tripled by 1997/1998, where contaminated sediments <TEL represented 43.85% of the entire lake area (although predominantly located in the eastern half). The influence of strong eastward circulation along the Ohio shoreline is apparent in the shape of the TEL isoline throughout the central basin in 1997/1998. By 2014, this contamination classification decreased in surface area representation to 38.62% while continually dominating the eastern half of Lake Erie. The dividing line between sediments ≥TEL to <PEL and <TEL through the middle of the central basin reflects a larger scale duality of land use, economies, and population density between Canada and the United States [63,64].

A complex dynamic of environmental policies has shaped navigational dredging and harbor development practices throughout Lake Erie since the 1970s. Prior to the enactment of the River and Harbor and Flood Control Act of 1970 [65] routine dredging of sediments from shipping routes by the US Army Corps of Engineers (USACE) resulted in open water dumping of dredged materials into Lake Erie. Since 1994, the State of Michigan has banned open water disposal of dredged materials, including contaminated sediments [65]; 55% of dredged materials are placed in near-shore or upland disposal facilities, 44% is housed in confined disposal facilities (CDF) and 1% of uncontaminated dredged sediments are disposed of in open waters [65]. From the mouth of the St. Clair River to its border with Ohio, the State of Michigan operates five CFD in Lake Erie [65]. That being said, the Detroit River continues to be the primary source of non-point source pollution to the lake [4].

Approximately 1.5 million tons of sediment are dredged annually from the Ohio shoreline and harbors (OEPA, 2016). In stark contrast to Michigan, the State of Ohio dumps 44% of all dredged materials into the open waters of Lake Erie [65]. Several offshore disposal locations, including Toledo, Sandusky, and Fairport (approximately 45 km east of Cleveland) were identified to contain Pb contaminated sediments ≥PEL from the 1971, and 2014 sediment surveys. Open lake disposal of dredged harbor sediments will be prohibited in the State of Ohio after July 2020 [66]; until then, contaminated sediments along the southern shoreline of Lake Erie will be continuously disturbed, increasing the rate and quantity of sediment resuspension and transportation throughout the lake.

5.2. Multivariate Geovisualization

Patterns of polluted sediments and their transport fate were given additional geophysical content by overlaying contamination layers and average circulation directions on top of the bathymetric data. When viewed in two-dimensions (2D) (Figures 13–15), the Pelee-Lorraine Sill and Long Point-Erie Sill are indistinguishable from other features throughout the lake basin. From the 1971 3D geovisualization, sediment transport from the western to central basin appears to be constrained by the Pelee-Lorraine Sill. The 1997/1998 and 2014 3D geovisualizations show sediments being transported eastward around Pelee Island and its ridge towards the central basin. The Long Point-Erie Sill presents another potential barrier to sediment movement. The strongest current along the southern shoreline of Lake Erie flows towards the eastern basin through a narrow channel south of the sill.

The 1971, 1997/1998, and 2014 3D geovisualizations display low Pb contamination values along the elevated sill and increasing levels of contamination aligned with the average circulation direction along the southern shoreline near Erie, PA.

When viewed in 2D, the contamination maps of Lake Erie neglect to inform the user of underlying geophysical characteristics of the lake basin. In 3D, bathymetric contours are illuminated from one perspective and shaded from another, encouraging the intuitive perception of changes in depth, slope, and orientation based on changing color contrast. The interpolated contamination maps from the 1971, 1997/1998, and 2014 sediment surveys are a valuable visual analytics tool for remediation efforts and contamination monitoring. Especially in the case of Cleveland Harbor, remediation resources can be efficiently allocated to regions of the lake that pose the greatest risk to the health and well-being of human and aquatic life. The water and sediments of Lake Erie know no political bounds. The entire basin is at risk of sediment contamination as long as shoreline regions operate to varying environmental standards.

There are two primary source areas that contribute to the observed Pb contamination patterns. Lead enters the system from the western Erie corridor (representing loadings from the Detroit River, Lake St. Clair, and the upstream lakes) moves south through the western basin and then predominately east along the southern Lake Erie-Ohio shoreline. As a result, particulates with associated Pb contamination settle out along a decreasing contamination gradient moving west-to-east, which is clearly evident from the kriging figures. In addition, Pb loadings enter Lake Erie via rivers/tributaries discharging from historically industrialized areas along the Ohio shoreline and are subject to the same circulation pattern as the material from the western Erie corridor as the cumulative contamination moves east.

In 3D, the Pelee-Lorraine Sill appears as a barrier to sediment transport from the western to central basins in the 1971 geovisualization. In both the 1997/1998, and 2014 geovisualizations, sediments are transported eastward around Pelee Island and its ridge, along the Ontario shoreline near Point Pelee and into the central basin. The Long Point-Erie Sill presents another potential barrier to sediment movement. The strongest lake current along the southern shoreline of Lake Erie flows towards the eastern basin through a narrow channel south of the sill. The 1971, 1997/1998, and 2014 3D geovisualizations display low Pb contamination values along the elevated sill; increasing levels of contamination aligned with the average circulation direction along the southern shoreline near Erie, Pennsylvania.

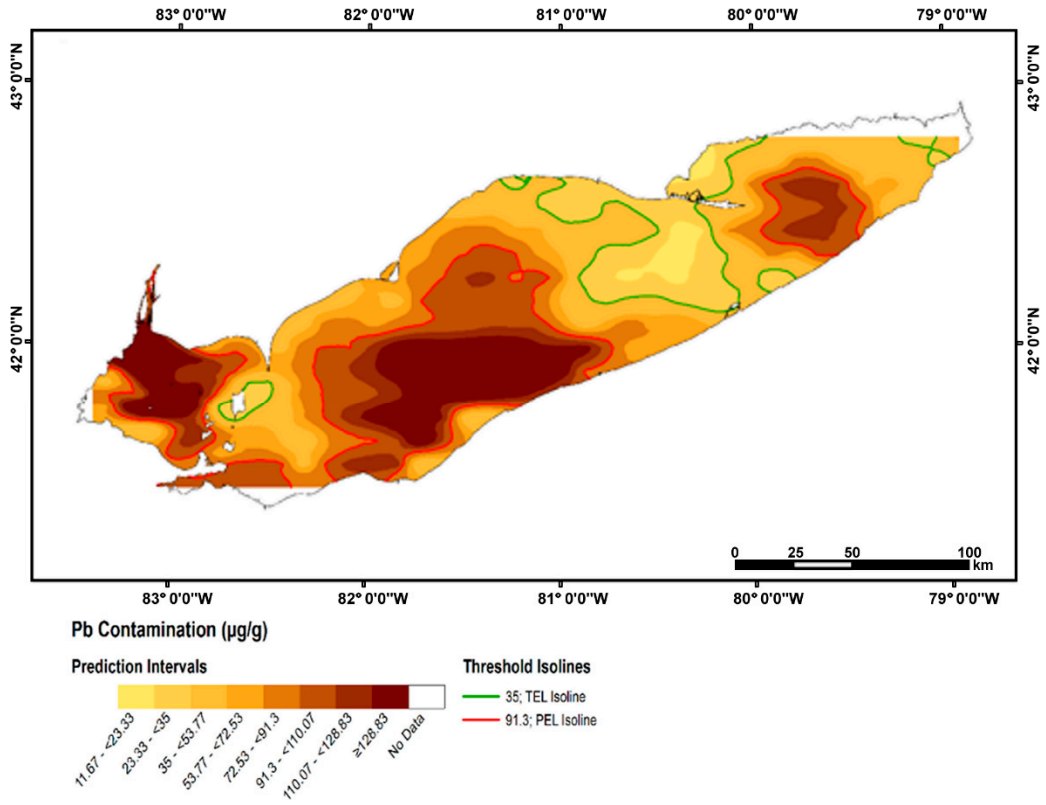

Figure 13. Kriging results of the 1971 Pb (log-normal) contamination in Lake Erie.

The steep sloping bathymetry into the middle of the eastern basin is also masked by 2D visualizations of the lake basin. When visualized in 3D, complex depth contours are revealed throughout the eastern basin with multiple levels of rapid changes in bathymetry. At the junction of the Long Point-Erie Sill with the Long Point Spit, and along the Ontario shoreline, very steep slopes (>89°) plunge to a maximum depth of 64 m. Along the New York state shoreline, the basins bathymetry is stepped with gradual declines into the depths of the eastern basin. Contaminated sediments from all sampling surveys were predicted to be located on the gentler slopes of the eastern basin. Sediments along the steepest sides of the eastern basin are likely very unstable due to greater gravitational and erosional forces acting upon the steep slopes [35,36].

There are various factors that generate Pb deposition to the Lake Erie: a combination of non-point sources in the watersheds and atmospheric deposition. The major factor related to a reduction in Pb pollution inputs in the Great Lakes was the phase out of leaded gasoline in the 1970s. Lead is typically strongly sediment-bound, especially for those sediments high in total organic carbon (TOC). Historical Pb contamination is associated with heavily industrialized areas and their associated pockets of contaminated sediment. It also resides in soils and on impervious surfaces [67] and can therefore enter the lake during snowmelt and storm events. Lead is still used in some industrial applications, including the automotive industry, so it can be assumed that there are some loadings from contemporary industrial activities in the western Erie corridor and along the Ohio shoreline, in addition to inputs from atmospheric deposition in the upper Great Lakes and Lake Erie itself.

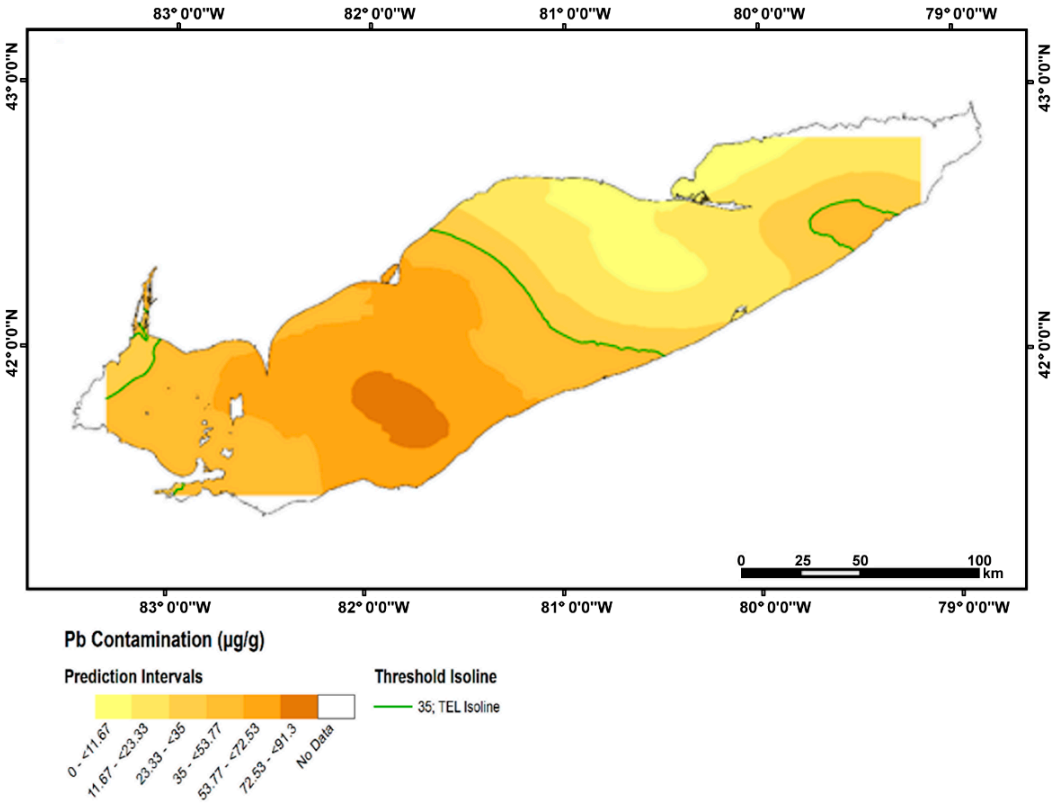

Figure 14. Kriging results of the 1997/1998 Pb (log-normal) contamination in Lake Erie.

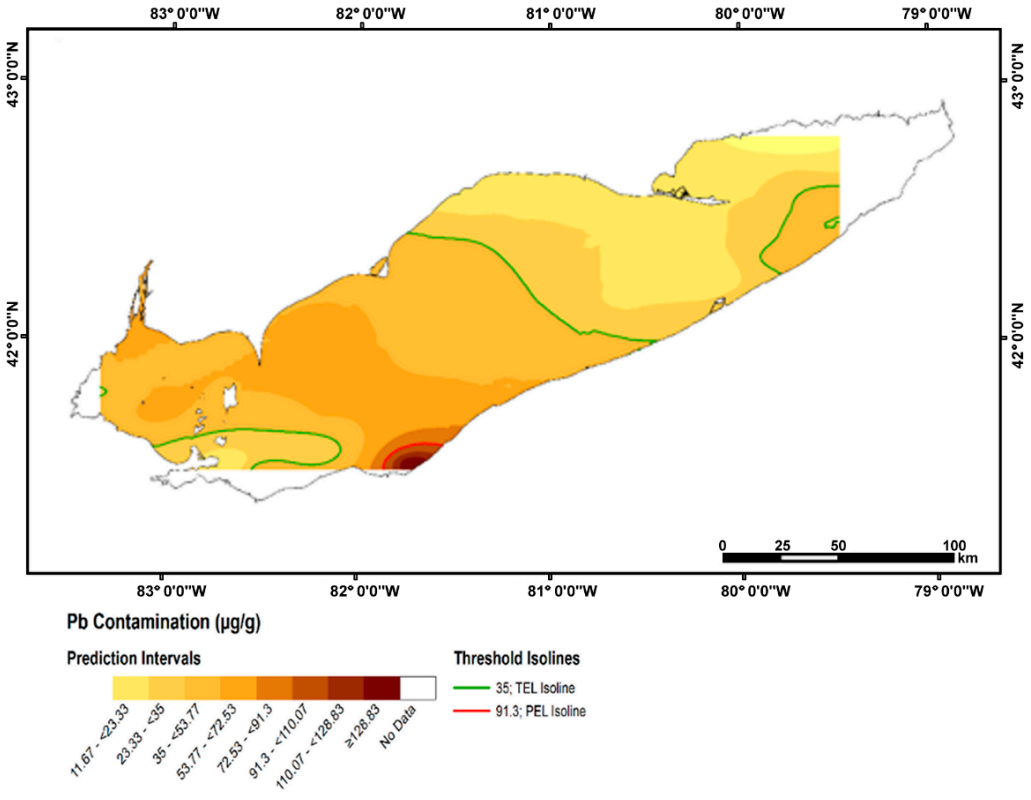

Figure 15. Kriging results of the 2014 Pb (log-normal) contamination in Lake Erie.

Maps and 3D geovisualizations are excellent tools for communicating spatial trends to a wide variety of individuals, ranging from the general public to scientists and government

officials. Sediment samples are a snapshot of contamination levels in a specific location at a certain time. In point form, the value of sediment contamination data to pollution control efforts and scientific communication is hindered by the disjunctive and incomplete nature of traditional dot and/or proportional circle maps. Spatial interpolation methods, like kriging, are the first step to enhancing the communicative value of contamination information from point data to a continuous data layer.

6. Conclusions

Improvements to Lake Erie sediment contamination have been largely driven by improvements to environmental policies (USAEC, 2012). The overall decrease in highly contaminated sediments ≥PEL in 1997/1998 corresponds with the phasing out of leaded gasoline throughout the 1990s. Although sediments posing the greatest health risk to humans and aquatic life have been virtually eliminated by 2014, sediments ≥TEL to <PEL dominate nearly half of the lake area and have the potential to pose environmental and health risks.

The research methodologies created through these geospatial analyses may help to bridge the knowledge gap between Great Lake experts and Great Lake citizens. Every three years, the International Joint Commission (IJC) reports on the Status of Great Lakes Ecosystem Integrity, holds a public forum, and reports on the progress towards binational commitments under the Great Lakes Water Quality Agreement (GLWQA) [68]. Maps and research available to the general public allow individuals to educate themselves on the evolving status of Great Lakes sediment contamination, increasing informed public participation at triennial IJC public forums. Research methodologies integrating ancillary variables may be operationalized with any sediment contaminant, so long as sediment properties and bathymetric data are available for the lake under analysis. Moving forward, it is essential to create maps of as many persistent toxic chemicals and heavy metals as possible for each lake to develop a thorough and historically significant body of knowledge for mitigating Great Lakes sediment contamination into the future.

Author Contributions: Conceptualization, K.W.F., D.E.F., and C.H.M.; methodology, K.W.F., D.E.F., and C.H.M.; software, K.W.F., D.E.F., and M.W.M.; validation, K.W.F., D.E.F., R.R.S., M.W.M., and R.W.; formal analysis, K.W.F. and D.E.F.; investigation, K.W.F., D.E.F., C.H.M., R.R.S., and M.W.M.; resources, K.W.F., D.E.F., and M.W.M.; data curation, K.W.F., D.E.F., and C.H.M.; writing—original draft preparation, K.W.F. and D.E.F.; writing—review and editing, K.W.F., D.E.F., C.H.M., R.R.S., M.W.M., and R.W.; visualization, K.W.F., D.E.F., R.R.S., M.W.M., and R.W. All authors have read and agreed to the published version of the manuscript.

Funding: This research received no external funding.

Data Availability Statement: Publicly available datasets were analyzed in this study. These data can be found at: https://open.canada.ca/data (accessed on 24 January 2021).

Conflicts of Interest: The authors declare no conflict of interest.

References

1. U.S. Environmental Protection Agency (USEPA). Great Lakes Facts and Figures. Available online: https://www.epa.gov/greatlakes/facts-and-figures-about-great-lakes (accessed on 24 January 2021).
2. Great Lakes Commission (GLC). Lake Erie. Available online: https://www.glc.org/lakes/lake-erie (accessed on 24 January 2021).
3. Evers, D.C.; Wiener, J.G.; Driscoll, C.T.; Gay, D.A.; Basu, N.; Monson, B.A.; Lambert, K.F.; Morrison, H.A.; Morgan, J.T.; Williams, K.A.; et al. *Great Lakes Mercury Connections: The Extent and Effects of Mercury Pollution in the Great Lakes Region*; Biodiversity Research Institute: Gorham, Maine, 2011; Report BRI 2011–2018; Available online: http://www.briloon.org/uploads/Library/item/263/file/Great%20Lakes%20HG%20Connections.pdf (accessed on 24 January 2021).
4. Marvin, C.H.; Charlton, M.N.; Reiner, E.J.; Kolic, T.; MacPherson, K.; Stern, G.A.; Braekevelt, E.; Estenik, J.F.; Thiessen, L.; Painter, S. Surficial Sediment Contamination in Lake Erie and Ontario: A Comparative Analysis. *J. Gt. Lakes Res.* **2002**, *28*, 437–450. [CrossRef]
5. Mitchell, D.E.; Forsythe, K.W.; Marvin, C.H.; Burniston, D.A. Assessing Statistical and Spatial Validity of Sediment Survey Design and Sampling Densities: Examples from Lake Erie. *Water Qual. Res. J.* **2018**, *53*, 118–132. [CrossRef]

6. Mitchell, D.E.; Forsythe, K.W.; Marvin, C.H.; Burniston, D.A. Temporal Trends and Origins of Lake Erie Cadmium Contamination in Relation to Sediment Substrate Type Using Multivariate Kriging Analyses. *Int. J. Geospat. Env. Res.* **2019**, *6*, 1–21.
7. Painter, S.; Marvin, C.H.; Rosa, F.; Reynoldson, T.B.; Charlton, M.N.; Fox, M.; Lina Thiessen, P.A.; Estenik, J.A. Sediment Contamination in Lake Erie: A 25-Year Retrospective Analysis. *J. Great Lakes Res.* **2001**, *27*, 434–448. [CrossRef]
8. Wuana, R.A.; Okieimen, F.E. Heavy Metals in Contaminated Soils: A Review of Sources, Chemistry, Risks and Best. Available Strategies for Remediation. *Int. Sch. Res. Netw. Ecol.* **2011**, 402647. [CrossRef]
9. Khosh Eghbal, M.Z. Spatial Distribution of Sediment Pollution in the Khajeh Kory River Using Kriging and GIS. *Earth Sci. Res. J.* **2014**, *18*, 173–179.
10. Aliff, M.N.; Reavie, E.D.; Post, S.P.; Zanko, L.M. Anthropocene geochemistry of metals in sediment cores from the Laurentian Great Lakes. *PeerJ* **2020**, *8*, e9034. [CrossRef]
11. Kot-Wasik, A. Water Quality Control: Part III, Human Impact on Water Resources. 2005. Available online: https://chem.pg.edu.pl/documents/175289/4237055/WQC_Part3_%20Human%20impact%20on%20water%20resources.pdf (accessed on 24 January 2021).
12. Stephanson, L. Environment Canada's Gasoline Regulations: Discussion Paper Proposing Indeterminate Exemption for the Use of Leaded Gasoline in Competition Vehicles. Environment and Climate Change Canada. 2009. Available online: http://www.ec.gc.ca/lcpe-cepa/default.asp?lang=En&n=54FE5535-1&wsdoc=8E3C2E9B-38A8-461A-8EC3-C3AA3B1FD585 (accessed on 24 January 2021).
13. U.S. Environmental Protection Agency (USEPA). EPA Takes Final Step in Phaseout of Leaded Gasoline. Available online: https://archive.epa.gov/epa/aboutepa/epa-takes-final-step-phaseout-leaded-gasoline.html (accessed on 24 January 2021).
14. Forsythe, K.W.; Dennis, M.; Marvin, C.H. Comparison of Mercury and Lead Sediment Concentrations in Lake Ontario (1968–1998) and Lake Erie (1971–1997/98) using a GIS-based Kriging Approach. *Water Qual. Res. J. Can.* **2004**, *39*, 190–206. [CrossRef]
15. Beletsky, D.; Saylor, J.H.; Schwab, D.J. Mean Circulation in the Great Lakes. *J. Gt. Lakes Res.* **1999**, *25*, 78–93. [CrossRef]
16. National Oceanic and Atmospheric Administration (NOAA). Great Lakes Bathymetry. Available online: https://www.ngdc.noaa.gov/mgg/greatlakes/greatlakes.html (accessed on 24 January 2021).
17. Yuan, F.; Li, H.; Kakarla, R.; Kasden, C.; Yao, S.; Xue, B.; Sun, Y. Variability of sedimentary phosphorus fractions in the western and Sandusky basins of Lake Erie. *J. Gt. Lakes Res.* **2020**, *46*, 976–988. [CrossRef]
18. Graney, J.R.; Halliday, A.N.; Keeler, G.J.; Nriagu, J.O.; Robbins, J.A.; Norton, S.A. Isotopic Record of Lead Pollution in Lake Sediments from the Northeastern United States. *Geochim. Cosmochim. Acta* **1995**, *59*, 1715–1728. [CrossRef]
19. Soong, K.L. Versuche zur Adsorptiven Bindung von Schwermetall Ionen an Künstlichen Tongemischen. Ph.D. Thesis, University of Heidelberg, Heidelberg, Germany, 1974.
20. Jain, C.K.; Ram, D. Adsorption of Metal Ions on Bed Sediments. *Hydrolog. Sci. J.* **1997**, *42*, 713–723. [CrossRef]
21. Marvin, C.H.; Grapentine, L.; Painter, S. Application of a Sediment Quality Index to the Lower Laurentian Great Lakes. *Environ. Monit. Assess.* **2004**, *91*, 1–16. [CrossRef]
22. Agency for Toxic Substances and Disease Registry (ATSDR). Toxicological Profile for Lead. Available online: https://www.atsdr.cdc.gov/ToxProfiles/tp.asp?id=96&tid=22 (accessed on 24 January 2021).
23. Bai, X.; Wang, J.; Schwab, D.J.; Yang, Y.; Luo, L.; Leshkevich, G.A.; Lui, S. Modeling 1993–2008 Climatology of Seasonal General Circulation and Thermal Structure in the Great Lakes Using FVCOM. *Ocean Model.* **2013**, *65*, 40–63. [CrossRef]
24. Rao, Y.R.; Schwab, D.J. Transport and Mixing Between the Coastal and Offshore Waters in the Great Lakes: A Review. *J. Gt. Lakes Res.* **2007**, *33*, 202–218. [CrossRef]
25. Essex Region Source Protection Area (ERSPA). State of Climate Change Research in the Great Lakes Region. Available online: https://essexregionconservation.ca/wp-content/uploads/2018/04/chapter-6-state-of-climate-change-research-in-the-great-lakes-region.pdf (accessed on 24 January 2021).
26. Morang, A.; Mohr, M.C.; Forgette, C.M. Longshore Sediment Movement and Supply along the U.S. Shoreline of Lake Erie. *J. Coast. Res.* **2011**, *27*, 619–635. [CrossRef]
27. Blais, J.M.; Kalff, J. The Influence of Lake Morphometry on Sediment Focusing. *Limnol. Oceanogr.* **1995**, *40*, 582–588. [CrossRef]
28. Canadian Council of Ministers of the Environment (CCME). *Climate, Nature, People: Indicators of Canada's Changing Climate*; Climate Change Indicators Task Group of the Canadian Council of Ministers of the Environment: Winnipeg, MB, Canada, 2003.
29. Verma, S.; Bhattarai, R.; Bosch, N.S.; Cooke, R.C.; Kalita, P.K.; Markus, M. Climate Change Impacts on Flow, Sediment and Nutrient Export in a Great Lakes Watershed Using SWAT. *Clean Soil Air Water (CSAWAC)* **2015**, *43*, 1445–1558. [CrossRef]
30. Fujisaki, A.; Wang, J.; Hu, H.; Schwab, D.J.; Hawley, N.; Rao, Y.R. A Modeling Study of Ice-Water Processes for Lake Erie Applying Coupled Ice-Circulation Models. *J. Gt. Lakes Res.* **2012**, *38*, 585–599. [CrossRef]
31. Pincus, H.J. The motion of sediment along the south shore of Lake Erie. *Coast. Eng. Proc.* **1953**, *4*, 119–146. [CrossRef]
32. Alther, G.R. Transport of Dredged Sediments after Disposal Operational in Lake Erie. *Ohio J. Sci.* **1981**, *81*, 2–8.
33. Hawley, N.; Eadie, B.J. Observations of Sediment Transport in Lake Erie during the Winter of 2004–2005. *J. Gt. Lakes Res.* **2007**, *33*, 816–827. [CrossRef]
34. Duarte, C.M.; Kalff, J. Littoral Slope as a Predictor of the Maximum Biomass of Submerged Macrophyte Communities. *Limnol. Oceanogr.* **1986**, *31*, 1072–1080. [CrossRef]

35. Derosier, A.L.; Hanshue, S.K.; Wehrly, K.E.; Farkas, J.K.; Nichols, M.J. *Michigan's Wildlife Action Plan, Littoral Zones*; Michigan Department of Natural Resources: Lansing, MI, USA, 2015. Available online: https://www.michigan.gov/documents/dnr/05_wap_littoral_zones_500065_7.pdf (accessed on 24 January 2021).
36. Christopherson, R.W.; Birkeland, G.H. *Geosystems: An Introduction to Physical Geography*, 9th ed.; Pearson: New York, NY, USA, 2015; pp. 1–688.
37. McCormick, B.H.; DeFanti, T.A.; Brown, M.D. Visualization in Scientific Computing. *Comput. Graph.* **1987**, *21*, 1–14. [CrossRef]
38. Andrienko, N.; Andrienko, G. Informed Spatial Decisions through Coordinated Views. *Inform.Visual.* **2003**, *2*, 270–285. [CrossRef]
39. MacEachren, A.M.; Gahegan, M.; Pike, W.; Brewer, I.; Cai, G.; Lengerich, E.; Hardisty, F. Geovisualization for Knowledge Construction and Decision Support. *IEEE Comput. Graph. Appl.* **2004**, *24*, 13–17. [CrossRef]
40. Koua, E.L.; Maceachren, A.; Kraak, M.-J. Evaluating the Usability of Visualization Methods in an Exploratory Geovisualization Environment. *Int. J. Geogr. Inf. Sci.* **2006**, *20*, 425–448. [CrossRef]
41. Rinner, C. A Geographic Visualization Approach to Multi-Criteria Evaluation of Urban Quality of Life. *Int. J. Geogr. Inf. Sci.* **2007**, *21*, 907–919. [CrossRef]
42. Ruda, A. Spatial decision support using data geo-visualization: The example of the conflict between landscape protection and tourism development. *J. Maps* **2016**, *12*, 1262–1267. [CrossRef]
43. Kumar, C.; Heuten, W.; Boll, S. Geovisualization for End User Decision Support: Easy and Effective Exploration of Urban Areas. In Proceedings of the GeoViz_Hamburg 2013: Interactive Maps That Help People Think, Hamburg, Germany, 6–8 March 2013; Available online: http://www.geomatik-hamburg.de/geoviz/online/Kumar_Abstract.pdf (accessed on 24 January 2021).
44. Lloyd, D.; Dykes, J. Human-centred approaches in geovisualization design: Investigating multiple methods through a long-term case study. *IEEE Trans. Vis. Comput. Graph.* **2011**, *17*, 2498–2507. [CrossRef]
45. Knust, C.; Buchroithner, M.F. Principles and Terminology of True-3D Geovisualization. *Cartogr. J.* **2014**, *51*, 191–202. [CrossRef]
46. Rukavina, N.; Dunnett, M.; Prokopec, C. Great Lakes Sediment Database. Environment and Climate Change Canada. 2013. Available online: http://www.ec.gc.ca/inre-nwri/default.asp?lang=En&n=9890771E-1 (accessed on 24 January 2021).
47. Forsythe, K.W.; Paudel, K.; Marvin, C.H. Geospatial analysis of zinc contamination in Lake Ontario sediments. *J. Environ. Inform.* **2010**, *16*, 1–10. [CrossRef]
48. Ouyang, Y.; Nkedi-Kizza, P.; Mansell, R.S.; Ren, J.Y. Spatial Distribution of DDT in Sediments from Estuarine Rivers of Central Florida. *J. Environ. Qual.* **2003**, *32*, 1710–1716. [CrossRef] [PubMed]
49. Forsythe, K.W.; Marvin, C.H. Assessing historical versus contemporary mercury and lead contamination in Lake Huron sediments. *Aquat. Ecosyst. Health Manag.* **2009**, *12*, 101–109. [CrossRef]
50. McBratney, A.B.; Webster, R. Choosing Functions for Semi-Variograms of Soil Properties and Fitting them to Sampling Estimates. *J. Soil Sci.* **1986**, *37*, 617–639. [CrossRef]
51. Forsythe, K.W.; Marvin, C.H. Analyzing the spatial distribution of sediment contamination in the Lower Great Lakes. *Water Qual. Res. J. Can.* **2005**, *40*, 389–401. [CrossRef]
52. Johnston, K.; Ver Hoef, J.; Krivoruchko, K.; Lucas, N. *Using ArcGIS Geostatistical Analyst*; ESRI: Redlands, CA, USA, 2001.
53. Simpson, G.; Wu, Y.H. Accuracy and Effort of Interpolation and Sampling: Can GIS Help Lower Field Costs? *ISPRS Int. J. Geoinf.* **2014**, *3*, 1317–1333. [CrossRef]
54. Forsythe, K.W.; Marvin, C.H.; Mitchell, D.E.; Aversa, J.M.; Swales, S.J.; Burniston, D.A.; Watt, J.P.; Jakubek, D.J.; McHenry, M.H.; Shaker, R.R. Utilization of Bathymetry Data to Examine Lead Sediment Contamination Distributions in Lake Ontario. *AIMS Environ. Sci.* **2016**, *3*, 347–361. [CrossRef]
55. Forsythe, K.W.; Marvin, C.H.; Valancius, C.J.; Watt, J.P.; Aversa, J.M.; Swales, S.J.; Jakubek, D.J.; Shaker, R.R. Geovisualization of Mercury Contamination in Lake St. Clair Sediments. *J. Mar. Sci. Eng.* **2016**, *4*, 19. [CrossRef]
56. Forsythe, K.W.; Marvin, C.H.; Valancius, C.J.; Watt, J.P.; Swales, S.J.; Aversa, J.M.; Jakubek, D.J. Using geovisualization to assess lead sediment contamination in Lake St. Clair. *Can. Geogr. Géogr. Can.* **2016**, *60*, 149–158. [CrossRef]
57. Forsythe, K.W.; Marvin, C.H.; Burniston, D.A.; MacDonald, M.W.; Watt, J.P. Geovisualization of Mercury Sediment Contamination in Lake Ontario. *AGIT J. Angew. Geoinform.* **2019**, *5*, 348–359.
58. Osburn, W.L. Geostatistical Analysis: Potentiometric Network for the Upper Floridian Aquifer in the St. Johns River Water Management District. 2000. Available online: ftp://secure.sjrwmd.com/technicalreports/TP/SJ2000-1.pdf (accessed on 24 January 2021).
59. Canadian Council of Ministers of the Environment (CCME). *Canadian Environmental Quality Guidelines*; Canadian Council of Ministers of the Environment: Winnipeg, MB, Canada, 1999.
60. Lui, X.; Wu, J.; Xu, J. Characterizing the Risk Assessment of Heavy Metals and Sampling Uncertainty Analysis in Paddy Field by Geostatistics and GIS. *Environ. Pollut.* **2006**, *141*, 257–264.
61. Gawedzki, A.; Forsythe, K.W. Assessing anthracene and arsenic contamination within Buffalo River sediments. *Int. J. Ecol.* **2012**, *2012*. [CrossRef]
62. *ArcGIS Version 10.5.1*; Environmental Systems Research Institute (ESRI): Redlands, CA, USA, 2017.
63. Murphy, R.E. Review of Megalopolis: The Urbanized Northeastern Seaboard of the United States. *Geogr. Rev.* **1962**, *52*, 452–454. [CrossRef]
64. Regional Planning Association (RPA). America 2050 Prospectus. 2005. Available online: https://rpa.org/work/reports/america-2050-prospectus (accessed on 24 January 2021).

65. Great Lakes and Ohio River Division, U.S. Army Corps of Engineers (USACE). Great Lakes System: Dredged Material Management Long Term Strategic Plan. Available online: https://www.lre.usace.army.mil/Portals/69/docs/Navigation/Great%20Lakes%20Dredged%20Material%20Management%20Long%20Term%20Strategic%20Plan.pdf (accessed on 24 January 2021).
66. Ohio Environmental Protection Agency (OEPA). Lake Erie Dredged Materials Program. Available online: https://www.epa.ohio.gov/dir/dredge.aspx (accessed on 24 January 2021).
67. Yang, H.; Shilland, E.; Appleby, P.G.; Rose, N.L.; Battarbee, R.W. Legacy Lead Stored in Catchments Is the Dominant Source for Lakes in the U.K.: Evidence from Atmospherically Derived ^{210}Pb. *Environ. Sci. Technol.* **2018**, *52*, 14070–14077. [CrossRef]
68. International Joint Commission (IJC). Great Lakes Water Quality Agreement. Available online: https://www.ijc.org/en/who/mission/glwqa (accessed on 24 January 2021).